Monthly Notices
of the
ROYAL ASTRONOMICAL SOCIETY

MNRAS **461,** 3399–3409 (2016) doi:10.1093/mnras/stw1373
Advance Access publication 2016 June 8

Transiting exoplanet candidates from *K2* Campaigns 5 and 6

Benjamin J. S. Pope,★ Hannu Parviainen and Suzanne Aigrain
Oxford Astrophysics, University of Oxford, Denys Wilkinson Building, Keble Rd, Oxford OX1 3RH, UK

Accepted 2016 June 3. Received 2016 June 1; in original form 2016 May 6

ABSTRACT

We introduce a new transit search and vetting pipeline for observations from the *K2* mission, and present the candidate transiting planets identified by this pipeline out of the targets in Campaigns 5 and 6. Our pipeline uses the Gaussian process-based K2SC code to correct for the *K2* pointing systematics and simultaneously model stellar variability. The systematics-corrected, variability-detrended light curves are searched for transits with the box-least-squares method, and a period-dependent detection threshold is used to generate a preliminary candidate list. Two or three individuals vet each candidate manually to produce the final candidate list, using a set of automatically generated transit fits and assorted diagnostic tests to inform the vetting. We detect 145 single-planet system candidates and 5 multi-planet systems, independently recovering the previously published hot Jupiters EPIC 212110888b, WASP-55b (EPIC 212300977b) and Qatar-2b (EPIC 212756297b). We also report the outcome of reconnaissance spectroscopy carried out for all candidates with *Kepler* magnitude $Kp \leq 13$, identifying 12 targets as likely false positives. We compare our results to those of other *K2* transit search pipelines, noting that ours performs particularly well for variable and/or active stars, but that the results are very similar overall. All the light curves and code used in the transit search and vetting process are publicly available, as are the follow-up spectra.

Key words: techniques: photometric – planetary systems – stars: variables: general.

1 INTRODUCTION

The *Kepler Space Telescope*, operated by NASA, has discovered the majority of known exoplanet candidates, with 4175 planet candidates identified over its 47-month nominal mission (Mullally et al. 2015). *Kepler* obtained high-precision (∼ tens of ppm) photometry of ∼170 000 stars over a field of view of 115 deg^2, identifying exoplanets by the characteristic repeated dip in brightness as they transit their host star (Borucki et al. 2010; Koch et al. 2010). After the failure of two of the four reaction wheels which formerly stabilized its pointing, it has been revived as the two-wheeled mission *K2*, using the two remaining wheels with the radiation pressure of the Sun to balance the third axis of rotation. *K2*'s observing sequence consists of a succession of ∼70–80 d 'Campaigns', each targeting a field in the ecliptic plane (Howell et al. 2014), with photometric precision comparable to that of the nominal *Kepler* mission (Vanderburg & Johnson 2014). As a result of the short Campaigns, *K2* is unable to detect planets with periods as long as were accessible with *Kepler*. On the other hand, by covering many different fields, it is able to search for short-period planets around a larger number of bright stars and to probe a wider range of environments.

K2 has diverse science goals (see Howell et al. 2014 for a more detailed discussion). It vastly increases upon the number of bright Sun-like stars and nearby late-type stars which were included in the *Kepler* prime mission. Short-period transiting planets discovered around these stars will be particularly good targets for future atmosphere studies. *K2* is also advancing stellar astrophysics through the study of pulsating stars, eclipsing binaries (EBs) and transients, as well as observing extragalactic and Solar system targets. By surveying fields located in or close to the Ecliptic plane, *K2* observations cover several nearby, young open clusters and associations, such as ρ Ophiuchi (ρ Oph) and Upper Scorpius (Upper Sco; Campaign 2), the Pleiades (Campaign 4), Praesepe (or the Beehive Cluster; Campaign 5), and Taurus and the Hyades (Campaigns 4 and 13). *K2* observations of these clusters are opening a new window on young star variability, including accretion-related variability, stellar activity and rotation, and pulsations, but also enable the discovery and characterization of young EBs and transiting planets. The latter are particularly important probes of the early stages of planetary evolution.

In this paper, we present a new pipeline to correct *K2* light curves for instrumental systematics and stellar variability, search them for planetary transit candidates and perform a series of diagnostic tests to weed out false positives. We apply this pipeline to Campaigns 5 and 6 (hereafter C5 and C6), identifying 77 and 71 single-planet

★E-mail: benjamin.pope@astro.ox.ac.uk

candidates among the 25 139 and 28 291 targets surveyed in each Campaign, as well as 5 systems showing multiple sets of transits. While our method is applicable to any *K2* light curve, and indeed readily adaptable to data from other instruments, a particular focus of its design has been to ensure good performance for young, variable stars, which represent a larger fraction of the most interesting targets for *K2* than for previous transit search missions.

K2 has already led to a number of noteworthy planetary transit discoveries, including disintegrating rocky planetesimals transiting a white dwarf (Vanderburg et al. 2015) and an M-dwarf (Sanchis-Ojeda et al. 2015), two unexpected additional planets in the hot Jupiter-hosting system WASP-47 (Becker et al. 2015), planetary companions to field M-dwarfs (Crossfield et al. 2015; Hirano et al. 2016b; Schlieder et al. 2016), transiting planets orbiting young stars in the Hyades and Upper Sco (Mann et al. 2016a,b) and many more individual planets. Several groups have also published catalogues of *K2* planet candidates, including Foreman-Mackey et al. (2015b, Campaign 1), Vanderburg et al. (2016, Campaigns 0 to 3), Crossfield et al. (2016, Campaigns 0 to 4) and Adams, Jackson & Endl (2016, Campaigns 0 to 5). In addition to this, Foreman-Mackey, Hogg & Schölkopf (2015a) and Osborn et al. (2016b) have presented systematic searches for single-transit events in *K*2, identifying long-period planet candidates. Where there is overlap, we will compare our results to these published catalogues.

The different pipelines used on *K2* data to date differ in subtle ways from each other, and from ours, at every stage of the light-curve detrending, transit search and vetting process, but particularly important differences are found in the light-curve extraction and detrending step. This is because of the importance of instrumental systematics (and, to a lesser extent, stellar variability) in *K2* data. In the *K2* mission, the *Kepler* satellite is balanced at an unstable equilibrium, using two reaction wheels and with solar radiation pressure keeping the third axis approximately steady. The third axis orientation must be maintained, however, by small thruster firings every ∼6 h, moving a typical star by of the order of ∼1 pixel across the detector, with the result that *K2* data contain significant pointing-related systematic photometric trends that make robust inference about the presence of planets more difficult than in the nominal *Kepler* mission. Several data-reduction pipelines have been developed by different groups to compensate for this effect (Vanderburg & Johnson 2014; Aigrain et al. 2015; Armstrong et al. 2015; Foreman-Mackey et al. 2015b; Lund et al. 2015), including our detrending pipeline (which we use in this paper; Aigrain, Parviainen & Pope 2016a, hereafter APP16). A unique feature of our approach is that systematics and stellar variability are modelled simultaneously rather than sequentially, which significantly improves the results when both effects are significant, especially on similar time-scales. The methods used in the remainder of our pipeline for transit search and vetting are relatively standard, but were implemented with particular attention to scalability and computational efficiency, and in such a way as to enable easy, uniform human vetting at the present time, as well as – in the future – progression towards a fully probabilistic assessment of the likelihood that individual candidates are *bona fide* planets.

The remainder of this paper is structured as follows. Sections 2, 3 and 4 describe our light-curve preparation, transit search and vetting methodology, respectively. Our catalogue of transiting planet candidates from C5 and C6 is given in Section 5, together with the results of preliminary spectroscopic reconnaissance. Section 6 gives links to the code used in our pipeline, all of which is publicly available, and we give our conclusions and discuss plans for future improvements in Section 7.

2 LIGHT-CURVE PREPARATION

K2 photometric time series are typically affected by sawtooth-like variations in measured flux, due to the drift and subsequent thruster reset of the spacecraft boresight roll angle. This effect, needed to maintain spacecraft pointing near the unstable equilibrium induced by solar radiation pressure, causes each star to move by of the order of ∼1 pixel over the course of each thruster-reset period of ∼6 h. This is translated into variations in flux by the differential sensitivity between pixels (inter-pixel variations) and across the surface of each pixel (intra-pixel variations), and by the loss of light outside the photometric aperture as it imperfectly matches and tracks the point spread function (aperture losses). Other systematic effects are also present (as they were in the light curves from the original *Kepler* mission), but the pointing-related variations are by far the most prominent. In addition to these instrumental systematics, the light curves also contain intrinsic stellar variability, most commonly due to the rotational modulation of star-spots. Both systematics and variability can severely hinder the detection of planetary transits, and must be filtered or modelled before the transit search can proceed.

The standard approach until now has been to do this sequentially, first modelling the systematics while ignoring the variability, then using some variation on a high-pass filter to remove most of the variability while preserving any planetary transits (the latter step exploits the fact that transits occur on shorter time-scales than most forms of stellar variability). However, this approach breaks down when both systematics and variability are of comparable amplitude, and occur on similar time-scales. While the typical rotation periods of *K2* target stars (days to weeks) are significantly longer than the ∼6 h characteristic time-scale of the pointing variations, there is none the less significant power in the variability of many stars on 6–12 h time-scales. This is particularly problematic for *K2*, which observes a larger fraction of young, rapidly rotating, active stars than earlier transit search missions. In such cases, modelling the systematics and variability simultaneously tends to be more effective, particularly if – as in the case of *K2* – the systematics can be constrained to depend primarily on the star's position on the detector, which should have no impact on its intrinsic brightness. This is the approach implemented in the K2SC pipeline (APP16), which uses a Gaussian process to model the systematics and variability simultaneously. The model contains two distinct components: the first depends on position only and represents the pointing-related systematics, and the second depends on time only, and represents the variability (plus any residual systematics not related to position). A sophisticated outlier rejection scheme is used to ensure that flares, eclipses and transits do not adversely affect the modelling, but are none the less preserved. We model the stellar variability one of two ways, either with the quasi-periodic exponential sine squared kernel in time (Rasmussen & Williams 2005) or with a squared exponential, and decide between the two by calculating a Lomb–Scargle periodogram (Lomb 1976) of the input light curve; if this shows a strong periodicity, we choose the quasi-periodic kernel. Otherwise, we represent stellar variability with a slowly varying squared exponential kernel.

We begin with the *K2* light curves available at the Mikulski Archive for Space Telescopes (MAST), which we process with K2SC to remove both systematics and variability. We exclude EPICs 200008644–200009280 in C5, which correspond to cluster superstamps (large contiguous regions of active pixels that cover star clusters) and to trans-Neptunian objects, and 200041889–200061149 in C6, which track Trojan asteroids. While cluster science is a key science goal of *K2*, standard MAST-pipeline aperture photometry

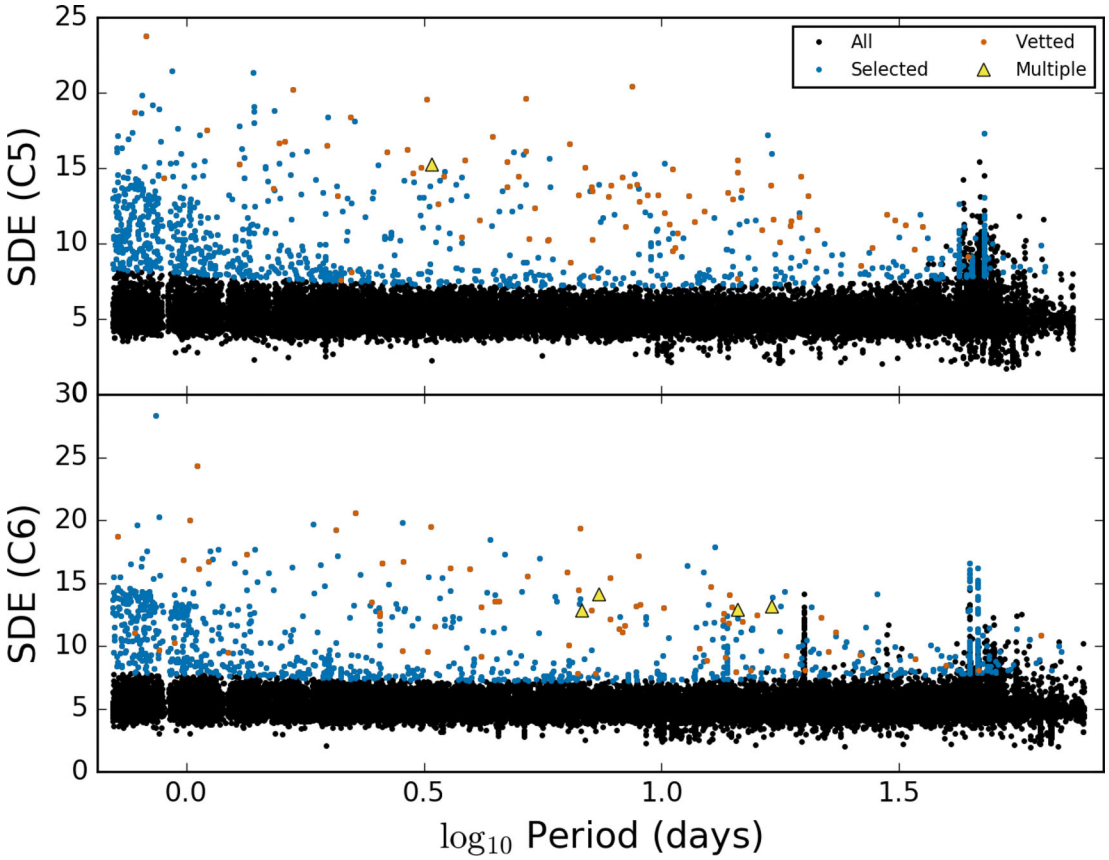

Figure 1. Initial selection of transit candidates based on the BLS detection statistic and period. We display SDE versus period for all objects in black, for C5 (top) and C6 (bottom). EPICs selected for visual examination (as described in Section 3) are shown in blue, and targets which pass the vetting process (described in Section 4) in orange. Yellow triangles display the first detected planet for the multiple-planet systems described in Section 5.1.

is not reliable in the extremely crowded fields of the cores of clusters, as are treated with superstamps. Many more widely distributed cluster members and probable cluster members outside the superstamp have MAST light curves; we exclude from the analysis presented here stars with very high cluster membership probability, in particular Praesepe stars (C5), as the subject of a separate study.

In APP16, we tested K2SC on both the simple aperture photometry light curves and light curves corrected for common-mode systematic trends by the *Kepler* presearch data conditioning (PDC) pipeline (Twicken et al. 2010; Smith et al. 2012; Stumpe et al. 2012). We found that the latter typically result in slightly improved photometric precision on transit time-scales (as measured using our proxy estimate of the 6.5 h combined differential photometric precision). This is most likely due to the fact that some of the common-mode trends removed by the PDC pipeline are related to variations in (e.g.) telescope focus and the temperature of various components, and not directly to the pointing, and are thus not modelled by K2SC. On the other hand, K2SC significantly improves the precision of PDC light curves, and enhances our ability to detect planetary transits (as demonstrated by APP16 using transit injection tests). We therefore use the K2SC-processed PDC light curves as our starting point for the transit search. The interested reader is referred to APP16 for more details on K2SC and its application to *K2* light curves.

3 TRANSIT SEARCH

Candidates are initially identified by a box-least-squares (BLS) algorithm (Kovács, Zucker & Mazeh 2002) which evaluates a signal-to-noise statistic, the signal detection efficiency (SDE), for a simple box-shaped transit for a grid of zero epochs spanning the Campaign and for periods ranging from 0.7 d to 98 per cent of the total duration of the Campaign, using our own version of the algorithm (Parviainen 2016). We apply this search to a Gaussian Process (GP) detrended light curve, which has been pre-whitened, where we subtract the GP time component to model smooth out-of-transit variations (Carpano, Aigrain & Favata 2003). We record the SDE, and best-fitting period, epoch and duration for each target.

Using this preliminary fit, we then fit a transit model using the PYTRANSIT package (Parviainen 2015), a fast implementation of the Mandel & Agol (2002) analytic transit light curves.

We use the BLS SDE to identify promising candidates for more detailed study. Using the injection test results from APP16 (fig. 10), we expect non-planet hosts to be distributed around a mean SDE of ∼6, roughly uniformly in log-period. In APP16, we therefore recommended a cut in SDE of ∼8 as a simple and effective way of selecting transit candidates. As is apparent in Fig. 1, in our real data, there is in fact some slope to this distribution, as well as a larger number of candidates at short periods.

In order to deal with this, we define an SDE threshold as a function of period. First, we discard single-transit as we consider these to be beyond the scope of this study, and examine the remaining objects. In preliminary inspection, we note that ∼65 long-period candidates in C6 result from systematics associated with particular pairs of bad epochs, leading to a pileup of candidates with poorly corrected light curves with zero epochs in two ∼0.5 d windows. We therefore identify these from a histogram of fitted BLS zero

epochs, and remove these candidates before proceeding. We also discard candidates for which the log-likelihood of a sinusoidal fit is greater than that of a transit, as a way of removing the most obvious variable sources. We then split the objects into 50 bins in period space, each containing an equal number of objects (469 for C5 and 457 for C6), thus using a variable bin size. In each bin, we find the median SDE, and the median absolute deviation-estimated standard deviation. Since there is a trend in the median as a function of period, we fit a second-order polynomial to the distribution of period as a function of median SDE, subtract this from each and find the standard deviation of the residuals. We then select for further analysis all candidates that lie more than 3σ above this value in each bin. We illustrate this in Fig. 1, displaying a plot of SDE versus period for both Campaigns, including all objects, selected objects and vetted objects.

4 VETTING

The procedure described in the previous section leads to a preliminary candidate list for each Campaign, which still contains both false detections caused by light-curve artefacts or other abnormalities, and astrophysical false positives, i.e. transit-like events which are not caused by a planet. To identify these and produce a cleaner candidate list, we visually inspect the light curves, along with a set of diagnostic plots based on transit model fits, broadly following the approach outlined in Batalha et al. (2010).

Some light curves are affected by poorly corrected systematics. These show residual ∼6 h variability which can lead to a spuriously large BLS detection statistic. We therefore systematically discard detections at the characteristic thruster firing period, and multiples thereof. Furthermore, the time component of the K2SC GP model does not always model very short period or high-amplitude stellar variability well. This is especially true for classical pulsators such as RR Lyr and Cepheid variables: while the overall variability pattern is modelled adequately, the extrema are not, leaving periodic dips in the residuals, which can lead to a high BLS statistic. Finally, while planetary transits and short-duration stellar eclipses are typically flagged as outliers by the K2SC model (so that they are left unchanged by the detrending process), the outlier flagging procedure is less successful for high-amplitude EBs where the eclipse duration exceeds a few per cent of the period. In those cases, the time component of the GP model partially reproduces the eclipses, leaving in the residuals shallow, periodic eclipse-like events which can superficially resemble planetary transits. All of these categories of false positive are readily identified by visually comparing the raw light curve, the systematics and time-dependent components of the K2SC GP model, and the detrended light curve.

EBs are the major source of false positives remaining after this step. The different types of EBs that can mimic a transit signal are discussed extensively in the literature (see e.g. Charbonneau et al. 2004 for an overview); we merely list them here: grazing EBs, EBs containing a large primary or small secondary star, and blended EBs (EBs whose eclipses are diluted by the light of a third star enclosed in the photometry aperture). To aid in the identification of such systems, we systematically produce, for all our candidates, a single-page report displaying key diagnostics in graphical and numerical form, as listed below. An example of such a report is shown in Fig. 2; the reports for all the candidates listed in Section 5 are provided online as supplementary material. The report shows, from top left to bottom right, the following.

(i) *Unfolded light-curve plots* showing the raw light curve, the systematics and time component of the K2SC GP model, and the detrended light curve used in the BLS transit search. The location of the transits is indicated by vertical dashed lines (if the light curve contains >20 transits, only the first 20 are marked).

(ii) *Main BLS and transit fit parameters* giving the BLS SDE detection statistic, the *Kp* magnitude of the target (magnitude in the *Kepler* bandpass) and the best-fitting parameters of a transit fit to the phase-folded detrended light curve.

(iii) *Folded transit plot* showing the best-fitting model overlaid on the phase-folded light curve.

(iv) *Even and odd transit plots* showing, in different colours, the binned phase-folded light curves for even- and odd-numbered transits (helpful in identifying nearly equal mass EBs where the BLS-detected period is half the true orbital period).

(v) *Individual transit plots* showing each transit (or the first 20 if the total number exceeds 20) separately (helpful in identifying false detections caused by light-curve artefacts).

(vi) *Secondary eclipse detection plots* showing the log-likelihood of a secondary eclipse with the same parameters as the best-fitting transit model, but variable depth, as a function of phase from 0.3 to 0.7 (EBs with low to moderate eccentricities but detectable secondary eclipses cause a clear peak in such a diagram).

(vii) *Per-orbit transit likelihood plot* showing the log-likelihood of the best-fitting transit model for each transit event separately (strong variations from one transit to the next indicate that the detection may be caused by or affected by light-curve artefacts).

(viii) *Full folded light-curve plot*: this can reveal secondary eclipses occurring outside the 0.3–0.7 phase range, or additional transit events.

(ix) *BLS periodogram* providing an additional means of assessing the significance of the detection (subsidiary peaks can also reveal additional sets of transits in the light curve).

All the transit model fits are performed using the PYTRANSIT package, which implements the analytic model of Mandel & Agol (2002). The parameters of the transit fits are epoch, period, planet-to-star radius ratio, impact parameter and stellar density. We also report the transit depth and duration, which are computed from the best-fitting transit model. Note that the transit models are evaluated with 3 min time sampling and binned up by a factor of 10 to account for the smearing of the ingress and egress caused by the relatively sparse sampling of *K2* long-cadence observations. The vetting process for transit candidates identified during the *Kepler* prime mission (see e.g. Batalha et al. 2010) also relies on the use of so-called 'rain diagrams': plots of flux versus *x*- and *y*-position of the target centroid. Such diagrams are highly effective at identifying blended EBs, where the target centroid can change significantly during eclipses (except for hierarchical triple system where the EB and contaminant are essentially co-located). In the case of *K2*, one must use the difference between the star's predicted position (based on the overall pointing variations of the satellite) and its measured centroid. We systematically produce such plots and use them in the vetting process, but they have not yet been incorporated into the single-page reports.

Any candidates which show clear signs of being false detections, or being caused by EBs, on the basis of the diagnostics described above, are discarded from the final candidate lists. Rather than define quantitative criteria for rejecting or keeping a candidate, at least two individuals vet all the candidates independently, and only those considered passable by all the vetters are retained. This clearly

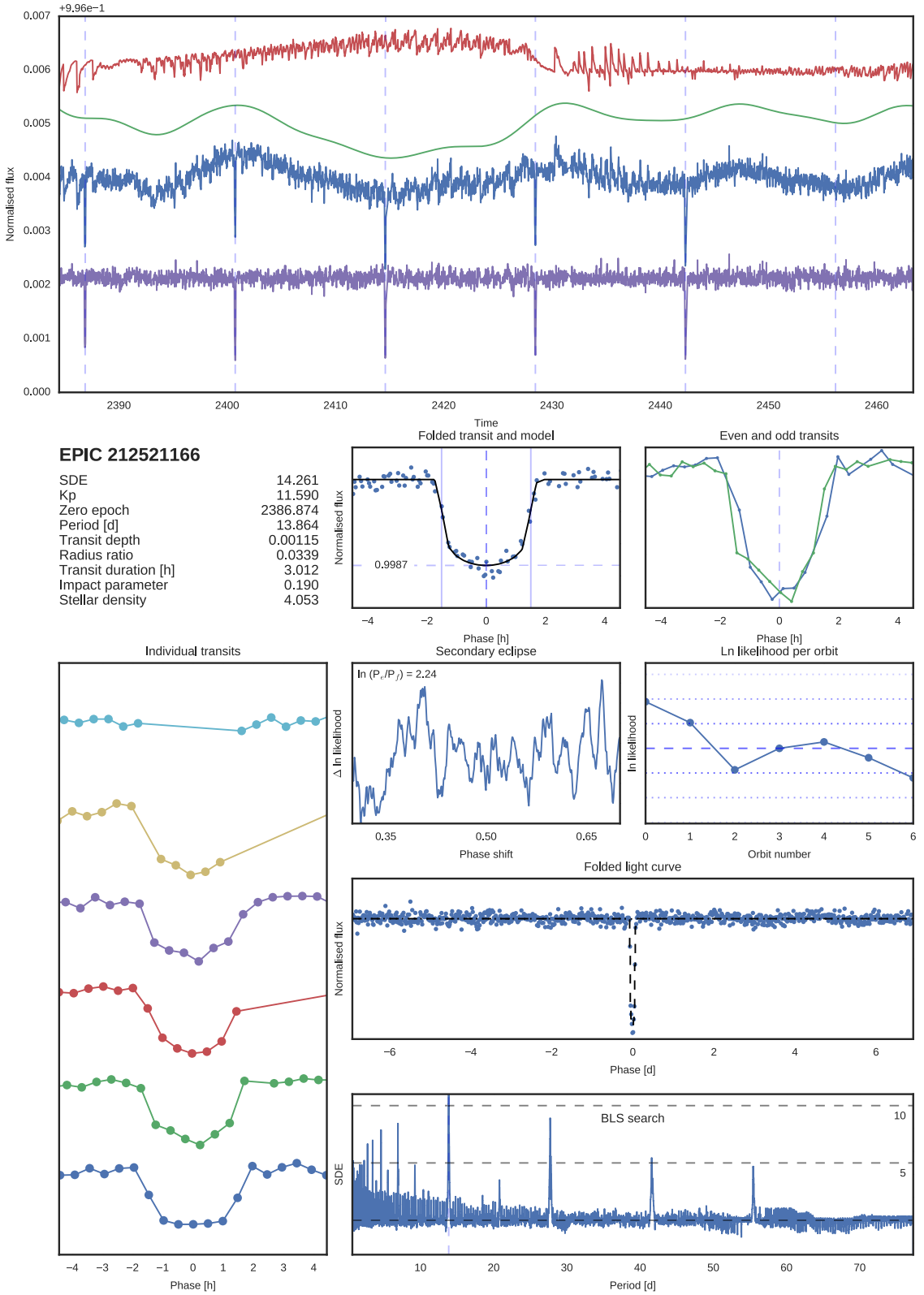

Figure 2. Example of a single-page vetting report for one of our candidates. See the text for details of the individual panels.

leaves scope for considerable improvement: ideally, we would like to perform a systematic, quantitative assessment of the probability that each candidate is indeed a planet, based on all the available information. One way to do this automatically is to use machine learning tools, such as the random forest algorithm recently implemented for *Kepler* (McCauliff et al. 2015), trained on transit candidate lists vetted by humans. However, this is beyond the scope of the present paper.

5 PLANET CANDIDATES

In Tables 1 and 2, we list the planet candidates that pass the tests described in Section 4, for C5 and C6, respectively. The last two columns give the number of reconnaissance spectra obtained for each candidate, where applicable, and the status of the candidate based on the spectra plus any other available information (see Section 5.2 for more details). The period and radius ratio of these candidates are displayed in Fig. 3. Out of 996 and 981 objects preselected for visual inspection in C5 and C6 respectively, we select 85 and 76 as *bona fide* candidates after vetting. A vetting diagnostic diagram similar to Fig. 2 is provided for each candidate in the supplementary online material.

Our C5 candidate list includes the hot Jupiter EPIC 212110888b, which has been independently discovered (from its *K2* light curve) and spectroscopically confirmed by Lillo-Box et al. (2016) and Hirano et al. (2016a). With an 0.8 per cent transit around an F9 star, the two publications agree on a mass of $M_{\rm p} \sim 1.7 \pm 0.1 M_{\rm J}$ and a radius of $1.4 \pm 0.1 R_{\rm J}$, differing within uncertainty according to the different stellar models. In addition to this, Osborn et al. (2016a) have obtained radial velocity (RV) spectroscopy of EPIC 212521166b, first reported by Aigrain, Parviainen & Pope (2016b), finding it to be a massive mini-Neptune with similar photometric parameters to those reported here.

Several long-period candidates were found around stars whose light curves display stochastic oscillations on time-scales of a few hours, and are hence likely to be red giants (EPIC 212411479, 212438212, 211996053 and 212481820). Although they did not explicitly fail any of the vetting tests, we did not include them in the final candidate lists, as it is difficult to distinguish a real transit from residuals from imperfectly modelled, stochastic stellar variability on the same time-scale. We note however that these events are in principle detectable, and might warrant more detailed study. While EPIC 211375488 and 212712473 show transit signals with high SDE, these objects are listed as galaxies in the EPIC catalogue and are excluded from the following analysis.

Our target sample partly overlaps with that of Adams et al. (2016), who searched for ultra-short-period planets (up to 1 d only) in Campaigns 0–5. Their report lists four candidates in C5: of these, we do not pre-select EPIC 211357309 or 211995325 for follow-up based on the BLS SDE, while we do pre-select 211685045 and 212150006. Both of the planets we miss have periods shorter than the 0.7 d cutoff we impose on our initial search. We did not include shorter periods in our search because both very short period pulsating stars and residual pointing systematics at $4c/d$ cause many false positives in that regime. EPIC 212150006 is listed in Table 1 as a *bona fide* planet candidate. Our light curve for 211685045 appears to show residual variability consistent with a false positive, so it was rejected at the vetting stage.

We have also compared our candidate list for both Campaigns to those kindly provided by Vanderburg (private communication). As we were coordinating our spectroscopic reconnaissance efforts, we shared our targets lists for magnitudes $Kp < 13$. Within that range, there is a very substantial overlap between our lists, with only a small number of objects found by one group but not by the other. In several cases, we have rejected candidates found by Vanderburg as having evidence for a secondary eclipse; in other cases, Vanderburg finds evidence of a secondary eclipse where we do not (see Comments in Tables 1 and 2). A few of our candidates were not detected by Vanderburg; these correspond to active stars whose variability and systematics are better modelled by the K2SC GP model than by piecewise polynomial detrending. Finally, we failed to detect a few of Vanderburg's candidates. In those cases, we see no evidence for a transit in our light curve, but the signal is clear in the K2SFF light curves. These are all bright stars, for which we suspect that the K2SFF photometric apertures are better suited to the point spread function than those used by MAST (Vanderburg & Johnson 2014).

This comparison shows that the different light-curve detrending, transit search and vetting processes are complementary, and that a more complete candidate list may be obtained by combining the results of several pipelines than by any single pipeline. We also note that the overall transit detection potential of *K2* may be best exploited by combining K2SFF aperture photometry (or similar) with K2SC detrending.

5.1 Multiple-planet systems

We also checked for additional transiting planets in the systems identified in Section 4. At the vetting stage, we made note of systems for which there was visual evidence of more than one set of transits. For each such system, we then subtracted the best-fitting model for the first set of transits and repeated the transit search and fitting on the residuals. The process was iterated until no further sets of transits were found.

We detect two sets of transits around each of EPIC 212012119 (C5); and 212393193, 212703473 and 212779596 (C6), and three sets of transits around 212768333 (C6). The parameters of these systems are presented in Table 3. For each of these systems, we provide a vetting diagnostic diagram similar to Fig. 2 for each set of transits separately in the supplementary online material.

EPIC 212651213 and 212651234 show two identical sets of transits which pass our initial vetting procedure, indicating a photometric blend. EPIC 212651213 was later found to be triple-lined (see Section 5.2), while 212651234 shows no RV variation over three epochs. We therefore conclude that EPIC 212651213 is an eclipsing SB3 system, and the apparent transits on 212651234 are the result of a photometric blend. These two systems are therefore not included in Table 3.

In addition to these, we detect three transit-like events with ∼3 to 5 per cent depth around EPIC 212656205, which do not have a periodic relation and have different depths. These may represent a planar hierarchical multiple stellar system, or multiple close-in giant planets.

5.2 Spectroscopic reconnaissance

For most of the objects in the EPIC catalogue (Huber et al. 2016), spectra have not previously been obtained and only photometric information is available. A single, moderate- to high-resolution spectrum can be used to determine the host star's spectral type and evolutionary stage, and to check for obvious signs of binarity (double- or triple-lined spectra). For single-lined, main-sequence cool stars, additional spectra can reveal km s^{-1} RV variations, indicative of a stellar or substellar companion. All our candidates which passed the vetting stage and were bright enough for efficient spectroscopic follow-up ($Kp \leq 13$) were observed at least once with the Tillinghast Reflector Echelle Spectrograph (TRES), at the 1.5 m Tillinghast Telescope on Mt Hopkins, Arizona. TRES has three spectroscopic resolving power settings available: 41 000 (high), 30 000 (medium) and

Table 1. Full list of our 86 vetted single-planet candidates in *K2* C5. RV semi-amplitude K (or limits) listed in Comments where applicable.

EPIC	RA	Dec.	V (mag)	$J-K$ (mag)	Period (d)	Epoch (BJD)	Depth (per cent)	$r_p/r_\star$ (per cent)	Duration (h)	Impact parameter	Density (g cm^{-3})	TRES (n)	Comments
211308899	08:53:18.006	+10:01:46.97	14.57	0.56	6.423	2457143.316	0.0395	1.9868	4.885	0.151	0.45		
211314705	08:36:31.182	+10:08:50.21	15.39	0.81	3.794	2457140.224	0.1007	3.1731	1.39	0	11.933	1	Hα emission
211319617	08:25:51.344	+10:14:49.08	12.6	0.47	8.866	2457143.397	0.1028	3.2056	2.679	0	3.893	1	OK
211328748	08:40:56.495	+10:25:20.56	9.96	0.3	17.178	2457139.95	0.0219	1.4808	2.452	0	9.833		
211331236	08:55:25.364	+10:28:08.87	14.65	0.86	1.292	2457140.193	0.1317	3.6291	1.153	0	7.162		
211333233	08:27:35.557	+10:30:23.62	9.95	1.04	5.409	2457142.885	0.0172	1.3096	2.344	0.028	3.544	1	Giant
211335816	08:26:29.764	+10:33:19.44	12.2	0.4	4.99	2457140.02	0.1907	4.3667	0.862	0.487	43.754	3	SB2
211336616	08:49:42.413	+10:34:13.95	13.1	0.62	44.13	2457149.28	0.0427	2.0655	4.635	0.037	3.731		
211342524	08:32:23.687	+10:40:38.06	12.42	0.35	14.449	2457149.367	9.1939	30.3214	0.595	0.991	1.38		
211351816	08:31:03.081	+10:50:51.31	12.61	0.66	8.406	2457142.05	0.0556	2.3577	5.668	0.205	0.367	1	Giant
211355342	08:30:12.968	+10:54:37.06	12.75	0.41	6.893	2457143.799	0.0585	2.4185	2.468	0	3.872	1	OK
211359660	08:40:43.278	+10:58:58.59	12	0.49	4.737	2457141.205	0.0977	3.1257	2.41	0.042	2.852	1	OK
211365543	08:29:48.825	+11:05:08.36	12.12	0.25	5.264	2457143.676	0.0096	0.9804	4.185	0.148	0.59		
211383821	08:44:09.925	+11:23:07.81	14.52	0.78	1.567	2457140.162	0.0326	1.8044	1.748	0.093	2.469		
211391664	08:25:57.189	+11:30:40.12	12.17	0.26	10.136	2457145.985	0.0869	2.9486	4.945	0.171	0.678	1	OK
211399359	08:32:16.114	+11:37:50.62	14.64	0.58	3.115	2457141.418	2.3415	15.3019	1.992	0.049	3.322		
211401787	08:27:35.269	+11:40:02.91	9.61	0.26	13.773	2457151.069	0.0245	1.5638	4.311	0.146	1.406	1	OK
211413752	08:54:50.291	+11:50:53.75	13.85	0.52	9.325	2457140.855	0.0923	3.0376	2.877	0	3.305		
211418729	08:31:31.911	+11:55:20.15	14.56	0.53	11.391	2457140.324	1.3265	11.5172	3.384	0.108	2.438		
211424769	08:35:24.644	+12:00:41.94	9.39	0.33	5.176	2457144.498	0.3485	5.9037	1.049	0.157	36.494	2	SB1
211428897	08:35:25.812	+12:04:33.04	14.09	0.79	1.611	2457140.661	0.0517	2.2748	1.059	0	11.471		
211439059	08:47:53.647	+12:13:54.85	13.29	0.51	18.641	2457146.51	0.0285	1.6896	5.22	0.173	1.057		
211442297	08:26:12.827	+12:16:54.97	13.36	0.38	20.272	2457157.159	1.4508	12.0449	3.141	0.101	5.435		
211490999	08:43:11.723	+13:00:34.53	13.6	0.43	9.844	2457146.33	0.0809	2.8435	3.425	0.118	2.026		
211491383	08:40:37.240	+13:00:52.83	11.78	0.33	4.144	2457141.601	0.0078	0.8845	2.717	0.101	1.722	1	OK
211509553	09:00:04.744	+13:16:25.94	16.58	0.8	20.359	2457151.414	3.3123	18.1997	2.938	0.131	6.602		
211525389	08:21:40.866	+13:29:51.11	11.75	0.45	8.267	2457139.723	0.1053	3.2454	3.216	0.139	2.038	1	OK
211529065	08:45:03.983	+13:32:59.40	13.78	0.6	4.4	2457142.979	0.1297	3.6012	1.456	0	12.033		
211562654	08:20:01.718	+14:01:10.06	12.85	0.46	10.792	2457147.782	0.0523	2.2862	3.581	0.151	1.916	1	OK
211569704	08:28:01.122	+14:07:10.62	12.36	0.72	34.023	2457156.994	0.0308	1.7559	3	0	10.625		
211579112	09:03:32.001	+14:15:01.90		0.86	17.703	2457156.427	0.6508	8.0674	1.872	0	22.768	1	OK
211586387	09:07:12.268	+14:21:19.71	14.64	0.65	35.383	2457142.906	0.0945	3.0738	3.094	0	10.078		
211594205	08:36:33.626	+14:27:42.97	10.35	0.54	16.994	2457148.501	0.0315	1.7749	2.285	0	12.012	1	OK
211645912	08:19:59.301	+15:10:40.42	12.62	0.37	10.673	2457140.54	0.0274	1.6562	3.436	0.104	2.185	1	OK
211713099	08:20:53.731	+16:05:27.41	13.83	0.4	8.562	2457141.15	0.4581	6.768	2.975	0.109	2.696		
211733267	08:40:02.259	+16:22:20.66	12.4	0.55	8.658	2457144.931	0.5656	7.5206	1.098	0.261	49.683	2	OK, $K \lesssim 100$ m s^{-1}[a]
211736671	08:13:31.650	+16:25:10.59	12.33	0.43	4.734	2457140.365	0.0778	2.7891	3.407	0.197	0.956	1	Giant
211743874	08:37:33.528	+16:31:19.57	12.57	0.3	12.281	2457148.217	0.0233	1.5248	3.876	0.151	1.72	1	OK
211763214	08:55:21.136	+16:47:39.05	12.73	0.5	21.199	2457146.569	0.0182	1.3507	4.283	0.123	2.224	1	OK
211770696	08:31:02.684	+16:54:02.04	12.41	0.38	16.271	2457145.973	0.0312	1.7668	7.534	0.223	0.298	1	OK
211770795	08:48:02.336	+16:54:06.67	14.88	0.67	7.728	2457141.099	0.0791	2.8133	2.83	0	2.88		
211770867	08:12:05.436	+16:54:10.82	12.28	0.3	27.693	2457147.872	1.8421	13.5722	6.343	0.465	0.636		
211779390	08:17:26.659	+17:01:27.68	13.45	0.72	3.85	2457141.528	0.0282	1.6802	1.627	0	7.553		
211783206	08:40:34.995	+17:04:40.57	14.6	0.65	7.134	2457146.467	0.045	2.1212	1.839	0	9.687		
211800191	08:51:32.348	+17:19:11.40	12.62	0.37	1.106	2457140.749	0.0975	3.1229	0.994	0	9.572	1	OK
211804579	08:36:16.266	+17:22:53.98	11.36	0.39	1.523	2457141.205	0.0605	2.4602	2.397	0.156	0.92		EB[b]
211808055	08:36:08.271	+17:25:48.30		0.4	3.383	2457142.603	0.1641	4.0506	3.721	0.353	0.46		
211814733	08:50:40.178	+17:31:29.61	11.21	0.57	14.71	2457145.892	0.4414	6.6437	2.382	0.079	9.096		
211816003	08:50:29.069	+17:32:32.80	13.84	0.49	14.452	2457144.86	0.1035	3.2178	3.32	0.228	3.077		
211818569	08:27:44.813	+17:34:45.83	13.32	0.69	5.186	2457143.561	1.0779	10.3821	1.778	0.133	7.584	2	OK, $K \lesssim 350$ m s^{-1}[c]
211834065	08:50:11.526	+17:47:57.57	11.81	0.29	10.545	2457142.426	0.0143	1.1974	3.259	0.164	2.469		EB[b,d]
211886472	09:08:31.807	+18:31:42.75	11.28	0.26	19.64	2457152.378	0.5501	7.4167	1.43	0.699	20.712		
211897691	08:40:19.814	+18:41:34.51	14.66	0.62	5.75	2457142.497	0.0945	3.0749	1.255	0	24.529		
211906259	08:45:14.646	+18:49:09.69	12.82	0.35	2.52	2457140.559	0.0105	1.0236	12.355	0.174	0.013		
211919004	08:39:06.491	+19:00:36.08	13.37	0.51	11.72	2457149.097	0.1051	3.2422	4.406	0	1.157		
211923431	08:31:44.965	+19:04:28.71	14.3	0.49	29.729	2457143.824	0.067	2.5878	4.998	0.196	1.895		
211924657	08:40:06.426	+19:05:34.36	16.25	0.81	2.645	2457141.999	0.2365	4.8634	1.404	0	8.086		
211929937	08:36:42.829	+19:10:25.72	14.43	0.52	3.477	2457142.412	1.7941	13.3945	2.205	0.016	2.743		
211941472	08:41:47.658	+19:20:50.99	11.95	0.39	5.78	2457143.635	0.0101	1.0064	3.138	0.154	1.525	1	OK
211945201	09:06:17.754	+19:24:08.11	10.15	0.31	19.491	2457158.827	0.1381	3.7166	3.369	0.035	4.29		
211965883	09:04:37.728	+19:42:52.51	14.63	0.82	10.555	2457146.496	0.1249	3.5337	1.307	0.3	34.611		
211969807	08:38:32.821	+19:46:25.78		0.86	1.974	2457140.376	0.1325	3.6401	1.407	0	6		
211990866	08:38:24.300	+20:06:21.83	10.65	0.28	1.674	2457140.72	0.0589	2.4261	1.398	0.218	4.832	1	OK
211993818	08:24:49.181	+20:09:10.78	7.34	0.47	8.986	2457140.043	4.8646	22.0558	0.002	1	0.24	3	SB2
211995398	08:14:37.512	+20:10:44.93			32.576	2457169.858	3.8336	19.5795	4.253	0	3.572		
212006318	08:42:00.319	+20:21:33.50	13.04	0.34	14.443	2457147.342	0.0245	1.5651	6.035	0.178	0.529	1	OK
212006344	08:25:54.315	+20:21:34.45	13.15	0.83	2.219	2457141.831	0.038	1.9484	1.118	0	13.438	1	Very Cool
212008766	08:37:07.785	+20:23:57.74	13.09	0.52	14.129	2457145.122	0.0854	2.9218	3.399	0	3.035	1	OK
212009427	08:31:29.870	+20:24:37.52		0.91	0.778	2457140.262	0.5428	7.3676	0.5	0.236	48.518		
212066407	08:39:21.244	+21:23:26.98	12.34	0.38	0.822	2457140.365	0.0437	2.0904	0.814	0.056	12.911	11	$K \sim 32.8 \pm 25$m s^{-1}

Table 1 – *continued*

EPIC	RA	Dec.	V (mag)	$J-K$ (mag)	Period (d)	Epoch (BJD)	Depth (per cent)	$r_p/r_\star$ (per cent)	Duration (h)	Impact parameter	Density (g cm^{-3})	TRES (n)	Comments
212069861	08:57:46.605	+21:27:12.72	14.78	0.85	30.953	2457147.496	0.1646	4.0566	3.236	0.152	7.442		
212088059	08:50:49.887	+21:47:20.84	15.61	0.88	10.366	2457141.715	0.124	3.5211	1.892	0	12.915		
212099230	08:32:17.657	+22:00:21.64	10.79	0.47	7.112	2457141.963	0.0585	2.418	2.651	0.009	3.222	1	OK
212110888	08:30:18.905	+22:14:09.27	11.45	0.34	2.996	2457141.351	0.6237	7.8978	1.971	0.068	3.292	5	HJ[d]
212130773	08:23:48.660	+22:38:02.48	14.63	0.61	18.711	2457151.886	0.1305	3.6132	5.972	0.162	0.713		
212132195	08:23:56.896	+22:39:46.96	12.03	0.63	26.198	2457164.39	0.0861	2.9347	3.173	0	6.919	1	OK
212136123	08:36:50.878	+22:44:28.04	15.09	0.5	2.226	2457140.262	0.0676	2.6003	1.679	0	3.986		
212138198	08:24:05.654	+22:46:59.84	13.21	0.58	3.209	2457142.373	0.2016	4.4905	0.725	0.131	69.121	1	OK
212141021	08:31:41.083	+22:50:30.01	13.55	0.57	2.918	2457140.099	0.0246	1.5674	1.914	0.066	3.499		
212150006	08:32:40.691	+23:01:55.20	14.77	0.51	0.898	2457139.982	0.1878	4.3334	0.958	0.122	8.524	5	[e]
212152341	08:51:00.966	+23:05:02.25			6.676	2457141.311	3.9424	19.8555	2.273	0.087	4.747		
212154564	08:54:33.884	+23:07:58.40		0.86	6.414	2457142.181	0.4643	6.8141	1.521	0.102	15.136		
212157262	08:50:05.666	+23:11:33.36	13.08	0.49	7.15	2457146.322	0.1068	3.2683	2.803	0.03	2.739	1	OK
212161956	08:25:29.502	+23:17:50.56	15.21	0.75	7.187	2457140.698	0.1195	3.4576	2.391	0	4.437		
212164470	08:39:15.271	+23:21:26.93	12.65	0.35	7.809	2457144.86	0.042	2.0497	3.403	0.204	1.572	1	OK

[a]RV measurements were 22.554 and 22.551 km s^{-1}, without uncertainties so assuming standard error.
[b]Vanderburg (private communication).
[c]RV uncertainties added in quadrature.
[d]Lillo-Box et al. (2016) and Hirano et al. (2016a).
[e]Adams et al. (2016).

20 000 (low); reconnaissance is typically conducted in the medium-resolution mode. In most cases, the RV precision achievable with TRES ($\sim$0.1 km s^{-1} or somewhat better) is not sufficient to detect the signal of a planetary-mass companion to a main-sequence star, except for hot Jupiters under favourable conditions.

Where possible, the systems were observed at or near quadrature in order to maximize the chances of resolving multiple sets of stellar lines. Any systems identified as giants, double- or triple-lined binaries based on the first observation were not observed any further. These are noted as 'GIANT', 'SB2' or 'SB3' in the final column of Tables 1 and 2. Additional spectra were taken near the opposite quadrature for some of the remaining single-lined candidates, if the planet-to-star radius ratio indicated that an orbital solution might be feasible with TRES. If the resulting RV change was too large for a planetary companion, the system was classified as a single-lined stellar binary (labelled 'SB1' in the tables). In the case of EPIC 212110888, which contains a hot Jupiter, further additional spectra were obtained in order to obtain a full orbital solution, which is consistent with the parameters published by Lillo-Box et al. (2016) and Hirano et al. (2016a), with TRES spectra best fitted by a 166 $\pm$ 21 RV semi-amplitude planet, with a mass of $1.18^{+0.15}_{-0.15} M_J$. One system (EPIC 212808289) may host a warm Jupiter, but additional spectra, ideally with better RV precision, are needed to confirm this. The inner planet in EPIC 212703473 is also a likely hot Jupiter. For EPIC 212066407 and 212803289, we list RV semi-amplitude K as determined by TRES, while for 211733267 and 211818569, with two epochs showing little variation we list upper limits on K. The remaining systems included in the TRES reconnaissance spectroscopy programme which were not found to show any evidence of binarity are simply noted as 'OK' in Tables 1 and 2. For the brightest among them, a full orbital solution might be feasible with dedicated high-precision RV instrument; otherwise a statistical evaluation of the likelihood that the companion(s) is/are indeed planetary ('validation') could be performed based on all the information available to date plus high spatial resolution imaging.

Overall, the TRES reconnaissance programme enabled us to rule out 8 out of the 85 single-planet candidates from C5, and 2 out of the 70 from C6, as giants or spectroscopic binaries, for a final total of surviving 145 single-planet candidates across both Campaigns.

6 SOURCE CODE AND DATA PRODUCTS

In the interests of open science, we have our code implementing the methods described in Sections 2, 3 and 4 publicly available. It consists of several open source packages distributed under a GNU Public License (GPL) v3 license. We invite interested readers to use, modify and contribute to this code as an evolving resource for the astronomical community. The K2SC systematics correction code (APP16) is available on GitHub at https://github.com/OxES/k2sc, the transit modelling code PYTRANSIT (Parviainen 2015) at https://github.com/hpparvi/PyTransit, and the code used to carry out the BLS transit search and produce the candidate reports, K2PS, is available at https://github.com/hpparvi/k2ps.

The data used and produced in the course of this paper are also publicly available. The full set of K2SC-processed *K2* light curves is available at MAST (https://archive.stsci.edu/prepds/k2sc/), and the candidate reports used in the vetting process are provided with this paper (for surviving candidates only) as supplementary online material, and the TRES spectra of our candidates have been uploaded to the 'ExoFOP–K2' website (https://exofop.ipac.caltech.edu/k2/).

7 CONCLUSIONS

We have presented a new pipeline to search for transiting planet candidates in *K2* data, and reported the results of applying this pipeline to C5 and C6, together with reconnaissance spectroscopy of the brightest of our candidates. We recover known planets and identify false positives due to stellar-mass companions. We have made our code, light curves and diagnostic data products publicly available to facilitate confirmation and comparison, and look forward to comparing our results with future work using other methods.

We have compared our results to those by Adams et al. (2016), the only published catalogue which covers one of the Campaigns we have analysed (C5), as well as with the unpublished candidate list produced by A. Vanderburg for both C5 and C6. In both cases, our results are generally consistent. The two candidates identified by Adams et al. (2016) and not by ourselves lie outside our chosen period search range. In several cases, we identified candidates found by Vanderburg, but discarded them at the vetting stage. On the other

Table 2. Full list of our 71 vetted single-planet candidates in *K2* C6. RV semi-amplitude K (or limits) listed in Comments where applicable.

EPIC	RA	Dec.	V (mag)	$J-K$ (mag)	Period (d)	Epoch (BJD)	Depth (per cent)	$r_p/r_\star$ (per cent)	Duration (h)	Impact parameter	Density (g cm^{-3})	TRES (n)	Comments
212270970	13:51:09.957	−18:27:42.22	13.48	0.42	1.717	2457218.134	0.0086	0.9286	6.192	0.185	0.065		
212278644	13:48:29.897	−18:11:47.77	14.15	0.37	12.426	2457227.549	0.0431	2.077	4.923	0.213	0.821		
212297394	13:48:49.493	−17:36:35.66	14.42	0.55	5.213	2457222.483	0.0709	2.6618	2.422	0.07	3.078		
212300977	13:35:01.945	−17:30:12.78	11.75	0.38	4.466	2457220.529	1.5619	12.4977	3.095	0.203	1.198		WASP-55
212301649	13:25:50.914	−17:28:59.27	14.33	0.56	1.225	2457217.565	0.0224	1.4962	9.016	0.554	0.019		
212310244	13:52:18.702	−17:13:31.61	14.27	0.55	6.669	2457220.874	0.0213	1.4607	4.984	0.166	0.438		
212321305	13:38:34.080	−16:54:36.35	14.08	0.41	34.144	2457228.926	0.2836	5.3257	7.923	0.196	0.546		
212330265	13:53:31.110	−16:39:34.92		0.9	4.174	2457220.427	0.1013	3.1828	1.863	0.019	5.453		
212351026	13:26:44.850	−16:06:18.54	15.51	0.81	2.548	2457218.171	0.2483	4.9828	4.903	0.423	0.143		
212351405	13:26:39.104	−16:05:42.00	14.32	0.57	2.549	2457218.158	0.1961	4.4285	3.833	0.407	0.3		
212357477	13:28:03.992	−15:56:16.15	10.36	0.39	6.327	2457221.228	0.0322	1.7952	1.675	0.083	11.238	1	OK
212370106	13:25:05.248	−15:37:30.26	14.71	0.83	22.446	2457225.441	0.1546	3.9319	3.48	0.011	4.491		
212380207	13:21:25.496	−15:22:37.99	13.37	0.44	26.147	2457241.871	0.0568	2.3842	4.341	0.094	2.66		
212394689	13:34:29.110	−15:02:10.89	12.4	0.45	6.679	2457223.42	0.0655	2.5593	2.427	0.123	3.854	1	OK
212398508	13:34:30.927	−14:56:49.78	13.87	0.47	46.423	2457237.276	0.0681	2.6102	6.591	0.211	1.277		
212418133	13:33:12.426	−14:30:14.60	13.41	0.4	3.333	2457219.846	0.0268	1.6372	3.792	0.118	0.511		
212420823	13:16:23.936	−14:26:40.67	14.4	0.54	9.029	2457219.139	0.0682	2.6107	3.009	0.078	2.772		
212424622	13:29:19.541	−14:21:34.07	13.35	0.33	12.012	2457219.497	0.0315	1.7745	5.162	0.153	0.712		
212425103	13:37:28.700	−14:20:56.00	14.73	0.52	0.946	2457218.175	0.0301	1.7346	1.324	0.077	3.467		
212432685	13:37:11.711	−14:10:50.12	13.28	0.33	1.063	2457217.992	0.0231	1.5188	1.316	0.072	3.958		
212435047	13:28:31.373	−14:07:34.65	12.5	0.33	1.115	2457218.451	0.0151	1.2269	1.562	0.099	2.475	1	OK
212440430	13:36:08.544	−14:00:33.18	13.46	0.42	19.991	2457228.16	0.0542	2.3276	4.266	0.122	2.125		
212443973	13:40:02.135	−13:55:55.34	16.03	0.79	0.779	2457217.748	0.0369	1.9207	0.66	0	23.004		
212451091	14:05:53.119	−13:46:45.80	14.46	0.52	12.666	2457226.371	0.1876	4.3318	3.51	0.053	2.462		
212454160	13:34:32.944	−13:42:45.42	12.88	0.42	0.876	2457218.236	0.0146	1.2103	7.372	0.526	0.032		
212454422	13:14:12.755	−13:42:24.76		0.91	3.269	2457220.227	1.2473	11.1682	0.966	0	30.571		
212460519	13:34:11.169	−13:34:36.94	12.92	0.8	7.387	2457223.798	0.0858	2.9294	2.422	0.064	4.362	1	OK
212480208	13:41:27.239	−13:09:39.23	11.14	0.42	10.099	2457224.771	0.0179	1.3385	3.71	0.141	1.62	1	OK
212495601	13:15:39.034	−12:49:37.35	13.96	0.41	21.677	2457229.646	0.0605	2.4596	4.534	0.13	1.913		
212496592	13:26:33.402	−12:48:23.65	13.26	0.53	2.858	2457219.561	0.0275	1.6582	2.043	0.188	2.69	1	OK
212499835	13:49:40.470	−12:44:17.29	16.45	0.58	6.883	2457221.015	0.4417	6.6463	5.531	0.232	0.318		
212499991	13:29:57.305	−12:44:05.00	13.55	0.51	15.381	2457225.459	0.0542	2.3288	2.187	0	12.41		
212521166	13:49:23.888	−12:17:04.17	11.91	0.58	13.864	2457219.875	0.1147	3.3865	3.007	0.043	4.292	1	OK[a]
212529560	13:28:31.542	−12:06:26.34	14.09	0.3	8.121	2457219.08	0.0406	2.014	3.398	0.164	1.678		
212534729	13:42:55.909	−11:59:39.30	13.29	0.49	13.479	2457223.541	0.0222	1.4904	2.84	0.01	4.966	1	OK
212543933	13:46:36.559	−11:48:17.80	14.15	0.37	7.806	2457223.497	0.0477	2.1838	2.75	0.042	3.159		
212554013	13:48:18.812	−11:35:20.32	15.04	0.58	3.588	2457220.338	1.2649	11.2466	1.868	0.073	4.618		
212555594	13:46:19.746	−11:33:22.51	12.7	0.46	4.163	2457220.44	0.0245	1.5661	1.441	0	11.741	1	OK
212562715	13:28:40.302	−11:23:57.59	13.28	0.42	13.524	2457220.467	0.0533	2.3085	2.314	0.191	8.706	1	OK
212563850	13:23:23.646	−11:22:29.11	13.71	0.77	14.311	2457222.751	0.0689	2.6248	1.96	0	16.029		
212570977	13:43:36.335	−11:13:24.85	14.08	0.42	8.853	2457223.894	2.4303	15.5895	3.534	0.536	1.022		
212572439	13:37:45.619	−11:11:33.26	13.18	0.53	2.581	2457217.866	0.3992	6.3185	1.51	0.052	6.319	1	HJ[b]
212572452	13:37:46.022	−11:11:32.00		0.81	2.581	2457217.865	3.029	17.404	1.509	0.153	6.14		
212575828	13:40:38.328	−11:07:01.53	15.79	0.57	2.06	2457217.849	0.1344	3.6658	1.378	0	6.668		
212577658	13:55:00.806	−11:04:47.35	11.8	0.45	14.069	2457221.323	0.0302	1.738	3.023	0.056	4.277	1	OK
212579424	13:11:25.778	−11:02:33.19			6.373	2457221.769	1.7919	13.3861	1.902	0	7.816		
212580872	13:40:56.895	−11:00:33.47	13.25	0.46	14.786	2457224.262	0.1334	3.6518	4.117	0	1.788	1	OK
212586030	13:43:25.957	−10:53:48.92	12.02	0.65	7.785	2457220.882	0.0541	2.3269	1.568	0	17.048	1	OK
212587672	13:41:46.729	−10:51:44.75	12.49	0.32	23.226	2457237.044	0.0469	2.1656	3.038	0.399	5.382	1	OK
212592101	13:42:41.093	−10:46:06.70		0.86	4.545	2457217.55	0.6354	7.9711	1.047	0.221	30.975	1	Giant
212639319	13:18:18.754	−09:41:30.69	12.62	0.48	13.843	2457222.438	0.0781	2.7945	1.55	0.275	27.844	1	OK
212645891	14:01:05.526	−09:32:24.40	12.73	0.4	0.984	2457218.042	0.1628	4.0344	0.682	0.24	24.06		
212646483	14:06:39.170	−09:31:35.42	14.09	0.49	8.253	2457219.873	0.0845	2.9071	1.04	0.663	25.972	1	OK
212661144	13:56:56.001	−09:11:15.46	13.85	0.49	2.459	2457218.91	0.0739	2.7192	1.092	0.327	13.479		EB[b]
212672300	13:38:26.144	−08:55:37.74	12.91	0.31	39.699	2457243.008	0.0614	2.4786	7.367	0.273	0.746	1	OK
212679181	13:26:56.924	−08:45:46.85	12.99	0.86	1.055	2457217.551	0.0458	2.1401	0.517	0.243	58.735		
212688920	13:32:03.256	−08:31:53.33	14.18	0.5	62.841	2457220.233	5.3463	23.1222	2.023	0.818	12.203	1	Cool
212689874	13:19:19.563	−08:30:34.13	12.5	0.37	15.854	2457225.044	0.0902	3.0041	4.502	0.112	1.439		
212697709	13:26:37.247	−08:19:03.22	12.91	0.35	3.952	2457218.287	0.6205	7.8771	1.416	0.159	11.309	1	OK
212705192	13:30:25.305	−08:07:48.94	12.2	0.43	2.268	2457219.619	0.4633	6.8064	1.515	0.073	5.478	1	OK
212735333	13:29:34.479	−07:22:26.41	12.16	0.4	8.358	2457218.187	0.0515	2.2698	3.214	0.241	1.943	1	OK
212737443	13:36:53.207	−07:19:05.32		0.66	13.603	2457221.355	0.1212	3.481	2.76	0	5.457		
212756297	13:50:37.408	−06:48:14.42	13.42	0.73	1.337	2457218.11	3.1165	17.6536	1.507	0.641	1.538		Qatar-2b
212757601	13:52:37.115	−06:46:09.78		0.58	1.018	2457218.013	0.9794	9.8964	1.322	0	3.774		
212772113	13:32:53.284	−06:21:24.67	14.02	0.58	8.953	2457223.806	0.1178	3.4324	0.812	0.124	137.771		
212782836	13:39:07.134	−06:02:29.74	11.49	0.44	7.125	2457222.12	0.0153	1.2382	2.814	0.092	2.667		
212796016	13:41:10.488	−05:39:48.11	14.85	0.81	3.216	2457217.935	0.0308	1.754	1.343	0	11.218		
212803289	13:55:05.698	−05:26:32.88	11.15	0.3	18.25	2457233.823	0.1776	4.2143	10.868	0.343	0.1	3	$K \sim 50 \pm 28$m s^{-1}
212813907	13:47:19.838	−05:06:21.87	14.3	0.56	6.725	2457221.836	0.2425	4.9246	0.921	0.156	69.908		
212828909	13:29:00.385	−04:36:36.82	12.46	0.5	2.85	2457218.558	0.025	1.5815	1.33	0.132	9.965	1	OK

[a]Mini-Neptune (Osborn et al. 2016a).
[b]Vanderburg (private communication).

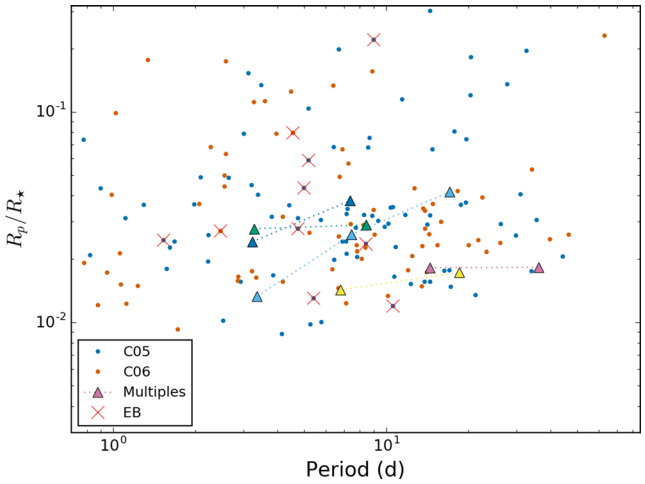

Figure 3. Radius ratio versus period for all vetted planet candidates from C5 (blue) and C6 (orange). Multiple systems are shown as triangles, with planets in each individual system sharing the same colour and joined by dotted lines. Objects which were found to be binaries following reconnaissance spectroscopy (see Section 5.2) are displayed with red crosses superimposed.

hand, we also failed to detect a few of his candidates altogether, and these correspond to the cases where the photometric precision of our light curves is not as good as that of the K2SFF light curves used by Vanderburg for the same object.

We also identify a small number of candidates, which were not reported by other teams. These are predominantly orbiting variable stars, which is consistent with our stated intention to write a pipeline that is particularly robust to astrophysical variability. More detailed comparison to other methods will become possible once more groups have published candidate lists for C5 and C6, and once we have processed earlier Campaigns, for which published candidate lists are already available.

Our results are broadly compatible with the K2SC injection tests presented in APP16, but a direct comparison is not feasible, as we have made some small but significant changes to our transit search methodology since. We will repeat the injection tests at a later date, after processing more Campaigns, to provide a quantitative assessment of the sensitivity of our final pipeline. There are a number of possible modifications to our pipeline that may yield improvements in sensitivity or reliability in the future. First, as noted above, for some bright stars our light curves are not as precise as those used by some other teams. We use the PDC-MAP light curves as our starting point; these are extracted using fixed, pixelized photometric aperture masks. For some types of stars (particularly bright stars, as noted in Vanderburg & Johnson 2014 and Lund et al. 2015), these apertures may not be optimal. Better sensitivity to shallow transits might be achieved by applying K2SC to light curves extracted using more optimized apertures. Another area where we hope to make progress in the near future is in making the vetting process more automatic, perhaps by implementing and training machine learning algorithms to distinguish between planetary transits and false positives.

Beyond the discovery of individual interesting systems, a significant element of the long-term legacy of the *K2* mission will be improved estimates of short-period planet incidence rates around types of stars which were relatively under-represented in the *Kepler* prime mission (such as M-dwarfs), as well as the ability to check for if the incidence of short-period planets depends in a measurable way on direction within the Ecliptic plane. By making all our code publicly available, we hope to facilitate the evaluation of such incidence rates, by providing all the tools needed for complete end-to-end simulations of the detection process.

ACKNOWLEDGEMENTS

We would like to thank Andrew Vanderburg for his correspondence in discussing our pipeline, comparing results and sharing information on possible false positive candidates. We would also like to thank Dave Latham for his helpful comments and his collaboration in TRES follow-up of our planet candidates. We are grateful for the efforts of the *Kepler* and *K2* teams, and in particular to Geert Barentsen for his help in answering some very detailed queries.

This research made use of NASA's Astrophysics Data System; the SIMBAD data base, operated at CDS, Strasbourg, France; and the IPYTHON (Pérez & Granger 2007) and SCIPY (Jones et al. 2001) packages. Some of the data presented in this paper were obtained from the Mikulski Archive for Space Telescopes (MAST). STScI is operated by the Association of Universities for Research in Astronomy, Inc., under NASA contract NAS5-26555. Support for MAST for non-*HST* data is provided by the NASA Office of Space Science via grant NNX13AC07G and by other grants and contracts.

Financial support for this work came from Balliol College, the Clarendon Fund, the Leverhulme Trust and the UK Science and Technology Facilities Council (STFC).

Table 3. Full list of our vetted multiple-system candidates. EPIC 212012119 is in C5, while the remaining objects are all from C6.

EPIC	RA	Dec.	V (mag)	$J-K$ (mag)	Period (d)	Epoch (BJD)	Depth (per cent)	$r_p/r_\star$ (per cent)	Duration (h)	Impact parameter	Density (g cm^{-3})	TRES (n)	Comments
212012119 b	08:48:40.775	+20:27:18.27	12.063	0.615	3.281	2457142.135	0.077	2.78	1.790	0	4.835	1	
c					8.438	2457142.495	0.084	2.90	2.029	0.266	7.643		
212393193 b	14:02:11.279	−15:04:10.34	11.92	0.32	14.452	2457219.472	0.0331	1.82	2.958	0	4.711	1	
c					36.152	2457236.741	0.0331	1.83	5.317	0.001	2.029		
212703473 b	13:24:56.770	−08:10:18.26	10.97	0.39	6.788	2457222.73	0.0204	1.4299	2.784	0.097	2.622	1	HJ Candidate
c					18.516	2457221.169	0.03	1.73	2.62	0.323	7.362		
212768333 b	13:15:22.515	−06:27:53.59	10.97	0.51	3.359	2457218.397	0.018	1.33	1.420	0.054	9.866	1	Low SNR
c					7.450	2457221.023	0.0681	2.61	2.610	0.003	3.539		Clear
d					17.043	2457221.61	0.1737	4.1673	2.581	0.066	8.305		Clear
212779596 b	13:55:36.409	−06:08:10.12	12.29	0.65	3.225	2457218.739	0.058	2.41	1.827	0.020	4.469	1	
c					7.374	2457222.93	0.1431	3.7832	2.316	0.13	4.887		

REFERENCES

Adams E. R., Jackson B., Endl M., 2016, preprint (arXiv:1603.06488)
Aigrain S., Hodgkin S. T., Irwin M. J., Lewis J. R., Roberts S. J., 2015, MNRAS, 447, 2880
Aigrain S., Parviainen H., Pope B. J. S., 2016a, MNRAS, 459, 2408 (APP16)
Aigrain S., Parviainen H., Pope B., 2016b, EPIC212521166: A Transiting Planet Candidate Discovered in Campaign 6 Data from the K2 Mission, Available at http://dx.doi.org/10.5281/zenodo.45873
Armstrong D. J. et al., 2015, A&A, 579, A19
Batalha N. M. et al., 2010, ApJ, 713, L103
Becker J. C., Vanderburg A., Adams F. C., Rappaport S. A., Schwengeler H. M., 2015, ApJ, 812, L18
Borucki W. J. et al., 2010, Science, 327, 977
Carpano S., Aigrain S., Favata F., 2003, A&A, 401, 743
Charbonneau D., Brown T. M., Dunham E. W., Latham D. W., Looper D. L., Mandushev G., 2004, in Holt S. S., Deming D., eds, AIP Conf. Ser. Vol. 713, The Search for Other Worlds. Am. Inst. Phys., New York, p. 151
Crossfield I. J. M. et al., 2015, ApJ, 804, 10
Crossfield I. J. M. et al., 2016, Am. Astron. Soc., Meeting Abstr. 227, 122.06
Foreman-Mackey D., Hogg D. W., Schölkopf B., 2015a, IAU General Assembly, 22, 2258352
Foreman-Mackey D., Montet B. T., Hogg D. W., Morton T. D., Wang D., Schölkopf B., 2015b, ApJ, 806, 215
Hirano T. et al., 2016a, preprint (arXiv:1602.00638)
Hirano T. et al., 2016b, ApJ, 820, 41
Howell S. B. et al., 2014, PASP, 126, 398
Huber D. et al., 2016, ApJS, 224, 2
Jones E., Oliphant T., Peterson P., Others 2001, SciPy: Open Source Scientific Tools for Python, Available at http://www.scipy.org/
Koch D. G. et al., 2010, ApJ, 713, L79
Kovács G., Zucker S., Mazeh T., 2002, A&A, 391, 369
Lillo-Box J. et al., 2016, preprint (arXiv:1601.07635)
Lomb N. R., 1976, Ap&SS, 39, 447
Lund M. N., Handberg R., Davies G. R., Chaplin W. J., Jones C. D., 2015, ApJ, 806, 30
McCauliff S. D. et al., 2015, ApJ, 806, 6
Mandel K., Agol E., 2002, ApJ, 580, L171
Mann A. W. et al., 2016a, ApJ, 818, 46
Mann A. W. et al., 2016b, ApJ, 818, 46
Mullally F. et al., 2015, ApJS, 217, 31
Osborn H. P. et al., 2016a, preprint (arXiv:1605.04291)
Osborn H. P. et al., 2016b, MNRAS, 457, 2273
Parviainen H., 2015, MNRAS, 450, 3233
Parviainen H., 2016, PyBLS: v0.9, Available at http://dx.doi.org/10.5281/zenodo.45604
Pérez F., Granger B. E., 2007, Comput. Sci. Eng., 9, 21
Rasmussen C. E., Williams C. K. I., 2005, Gaussian Processes for Machine Learning (Adaptive Computation and Machine Learning). MIT Press, Cambridge
Sanchis-Ojeda R. et al., 2015, ApJ, 812, 112
Schlieder J. E. et al., 2016, ApJ, 818, 87
Smith J. C. et al., 2012, PASP, 124, 1000
Stumpe M. C. et al., 2012, PASP, 124, 985
Twicken J. D., Chandrasekaran H., Jenkins J. M., Gunter J. P., Girouard F., Klaus T. C., 2010, Proc. SPIE, 7740, 77401U
Vanderburg A., Johnson J. A., 2014, PASP, 126, 948
Vanderburg A. et al., 2015, Nature, 526, 546
Vanderburg A. et al., 2016, ApJS, 222, 14

SUPPORTING INFORMATION

Additional Supporting Information may be found in the online version of this article:

suppl_data
(http://www.mnras.oxfordjournals.org/lookup/suppl/doi:10.1093/mnras/stw1373/-/DC1).

Please note: Oxford University Press is not responsible for the content or functionality of any supporting materials supplied by the authors. Any queries (other than missing material) should be directed to the corresponding author for the article.

This paper has been typeset from a TEX/LATEX file prepared by the author.